Environmental Research 214 (2022) 113774

Contents lists available at ScienceDirect

Environmental Research

journal homepage: www.elsevier.com/locate/envres

Effects of shrub-grass cover on the hillslope overland flow and soil erosion under simulated rainfall

Xiao Li [a,b], Yifan Zhang [a,b], Xiaodong Ji [a,b], Peter Strauss [c], Zhiqiang Zhang [a,b,*]

[a] Jixian National Forest Ecosystem Observation and Research Station, CNERN, School of Soil and Water Conservation, Beijing Forestry University, Beijing, 100083, PR China

[b] Key Laboratory of Soil and Water Conservation and Desertification Combating, State Forestry and Grassland Administration, PR China

[c] Institute for Land and Water Management Research, Federal Agency for Water Management, A-3252, Petzenkirchen, Austria

ARTICLE INFO

Keywords:
Shrub-grass community
Simulated rainfall
Overland flow
Soil erosion
Hydrodynamic parameters
Water-limited and highland regions

ABSTRACT

Vegetation plays a vital role in regulating hydrological cycle and controlling soil erosion at multiple spatial and temporal scales. Establishing shrub-grass community is one of the widely adopted practices to increase rainfall infiltration and reduce soil erosion in water-limited and highland regions. To understand the effects of such vegetation communities on soil erosion and overland flow under different rainfall regimes at the hillslope scale, we conducted rainfall simulation experiments by setting up parallel plots at fixed slope of 15° including unvegetated (coverage 0%), shrub only (coverage 50%), grass only (coverage 50%), and shrub-grass covered (coverages 25%, 50%, 75%, and 100%) and constant rainfall intensities of 30, 60, and 90 mm h^{-1} rainfalls lasting 60 min each after the initiation of overland flow. Two native species *Lespedeza bicolor* and *Carex giraldiana,* distributed in the soil sampling region were planted on the plots to achieve designed coverages. We found that the overland flow and sediment load from vegetated slopes were reduced by 9%–58% and 27%–98%, respectively, compared with unvegetated slopes while the infiltration rate increased by over 45%. Shrub-grass community reduced the overland flow and sediment yield more significantly than shrub only and grass only treatments with the same coverage of 50% under three rainfall intensities. In addition, the overland flow rate linearly decreased while the mean sediment yield exponentially reduced against the increase in shrub-grass community coverage. Hydrodynamically, shrub-grass communities not only increased the critical hydrodynamic forces for the initiating soil erosion but also increased the resistance coefficient leading to reduce overland flow velocity, stream power, and thus soil erosion from the vegetative slope even under extreme rainfalls. Our research highlights the importance of developing the shrub-grass communities to reduce the quantity and energy of overland flow and control soil erosion on the hillslopes in water-limited and highland regions.

1. Introduction

As a primary cause of land degradation, soil erosion is a critical ecological, environmental, economic, and social problem that has garnered increasing attention globally (Borrelli et al., 2017; Dlamini et al., 2011; Li et al., 2016; Mann et al., 2017). Soil erosion reduces the soil productivity, fragments the landscape, increases the streamflow sediment concentration, and pollutes the downstream water bodies, leading to the degradation of hydrological health and watershed ecosystem at different scales (Kervroëdan et al., 2018; Ruiz-Colmenero et al., 2013; Wu et al., 2017). Among various controlling measures on soil erosion from hillslopes such as engineering, biological, and management (Allton et al., 2007; Sun et al., 2019; Yan et al., 2018), vegetation restoration is one of the most important and widely used nature-based approaches (Cerdà, 2007; Espigares et al., 2011; Liu et al., 2014). Vegetation in general reduces soil loss by enhancing the interception of rainfall, reducing the kinetic energy of raindrops, improving soil aggregate stability and soil infiltration, increasing the roughness of the underlying surface, and dissipating overland flow energy (Mahmoodabadi and Sajjadi, 2016; Xin et al., 2016; Zare et al., 2016; Zuazo and Pleguezuelo, 2008). Mixed shrub and grass communities are widely distributed in water-scarce and highland regions and have great potential for contolling soil erosion. However, previous studies are often conducted to explore the effects of either shrub only or grass only covers

* Corresponding author. Jixian National Forest Ecosystem Observation and Research Station, CNERN, School of Soil and Water Conservation, Beijing Forestry University, Beijing, 100083, China.

E-mail address: Zhqzhang@bjfu.edu.cn (Z. Zhang).

https://doi.org/10.1016/j.envres.2022.113774
Received 22 January 2022; Received in revised form 14 June 2022; Accepted 27 June 2022
Available online 28 June 2022

on the overland flow generation and soil erosion (Chen et al., 2018; Liu et al., 2019; Xiao et al., 2017). The functionalities of mixed shrub and grass communities on the overland flow and soil erosion are not well documented. Therefore, it is essential to investigate the effects of such vegetation type on the generation of overland flow and soil erosion for developing sound vegetation restoration scheme and achieve soil erosion control objective for these regions.

A large number of previous studies have been conducted to explore the effects of either the grass or the shrub cover on the hillslope overland flow and soil erosion in water-limited and highland regions (Chen et al., 2018; Li et al., 2009; Liu et al., 2019; Wei et al., 2007; Xiao et al., 2017). Shrub plots have lower overland flow and soil erosion rates than bare plots under simulated rainfall on the Loess Plateau (Xiao et al., 2017). Sediment yield from field grass plots decreases rapidly as the coverage increased from 0% to 90% (Li et al., 2009). Well-covered shrubland and native grassland had better soil and water conservation benefits than woodland and pastureland in the semiarid Loess Plateau of China (Huang et al., 2006). Grassland generally shows a more effective controlling capacity on the overland flow and soil erosion than that of shrubland while less effective under short-duration heavy rainfall. The dense canopies of shrublands intercept rainfall and significantly reduce the raindrop energy and overland flow (Pizarro et al., 2006; Wei et al., 2007). However, the patchy distribution of shrubland could lead to soil erosion in areas without grass below the canopy of shrubs, as widely observed in the dryland regions (Arnaez et al., 2015). Combined shrub and grass communities might be a better choice for balancing the sediment yield reduction and overland flow production in semi-arid and highland areas (Liu et al., 2019; Wang et al., 2012). However, most previous studies involved only one single vegetation type, e.g., shrub-coverage or grass-coverage, the knowledge in quantifying the performance of sediment reduction and overland flow maintenance in mixed shrub-grass communities is relatively rare.

Hydrodynamic regulation by vegetation cover is critical to understand the overland flow generation and soil erosion on the hillslopes (Krause et al., 2017; Sun et al., 2019; Xu et al., 2006b; Zhang et al., 2006). Such regulations depend on the vegetation effects on the surface resistance, soil infiltration, flow quantity, and flow energy that drives the soil erosion as shallow open-channel flows (Mu et al., 2019; Wang et al., 2015, 2019; Zhang et al., 2013, 2017a). In general, the impacts in overland flow regime, flow depth, flow resistance, flow energy, and sediment concentration by different vegetations such as natural slope, bare land, grassland, and shrubland are well documented (Li et al., 2006, 2017; Martínez-Murillo et al., 2013; Xu et al., 2017). Overland flow rates of bare land slopes are 2.0–14.4 times higher than grassland and 2.6–6.6 times higher than shrubland (Yao et al., 2011). While the critical flow shear stress, critical stream power and critical unit energy of a cross-section of grassland and shrubland are 1.9–3.3, 3.5–4.7, and 1.4–1.7 times higher than that of bare land (Xiao et al., 2011a). Sediment transport rates increase linearly against such hydrodynamic parameters (Xiao et al., 2011a; Xu et al., 2017; Yao et al., 2011). Vegetation cover, in general, could significantly reduce the flow velocity and increase the Manning roughness coefficient. However, the resistance coefficient of shallow overland flow could decrease with an increasing Reynolds number at a low vegetation coverage while increasing linearly at high vegetation coverages (Wu et al., 2007; Zhang et al., 2014a). Rainfall regimes play a significant role in the hydrodynamics of overland flow. The stream power of overland flow could better reflect the dynamic process of hillslope erosion in these hydrodynamics parameters. The stream power and erosion amount remain stable at coverages ranging between 40% and 80%, which could be used as an index to evaluate the regulation effect of vegetation on erosion (Zhu et al., 2010). However, the hydrodynamic mechanism of the complex underlying surface conditions such as the combination of shrub and grass community under different rainfall intensities is not well investigated.

We, therefore, hypothesized that mixed shrub and grass community is more effective than grass only or shrub only coummunities to conserve soil and water at slope scale in water-limited and highland regions. Simulated rainfall experiments were performed on the slopes with different coverages of grass only, shrub only and mixed shrub-grass vegetation to: (1) quantify the overland flow and sediment yield against vegetation coverages, (2) explore the rainfall intensity on overland flow and sediment yield against different vegetation coverages, (3) understand the physical process of overland flow and soil erosion for these experiments in terms of hydrodynamics properties.

2. Materials and methods

2.1. Experimental design

Rainfall simulation experiments were carried out in an indoor permanent Rainfall Simulation Hall located in Jiufeng Experimental Forest Farm in Beijing, China. The large-scale automatic pendent simulator (QYJY-503C, Xi'an Qingyuan Measurement & Control Technology Co., Ltd, China) has a rainfall height of 12.0 m, covering 8.0 m × 8.0 m. The rainfall simulator consists of a controller, gauges, pumps, water pipes and sprinklers, as well as other components. The type of sprinklers is rotary downjet sprinkler. The rainfall process is automatically controlled through a computer console, and the uniformity of rainfall, which refects the unit weight of rainwater in diferent locations of the distribution of uniformity, was 0.85 ± 0.04. Constant rainfall intensity can be achieved from 10 to 300 mm h^{-1}. Raindrop diameters ranged from 0.70 mm to 3.50 mm, and terminal velocity error (compared with natural rainfall) of raindrops is approximately <0.50 m s^{-1} (Huo et al., 2015; Wang et al., 2021). The water supply source of rainfall simulation was urban tap water. In general, electrical conductivity has a positive correlation with electrolyte concentration in the solution (Kim and Miller, 1996; Yao et al., 2013), electrical conductivity of the tap water of our experiments 0.272 ± 0.082 mS cm^{-1} was similar with the natural rainfall 0.185 ± 0.116 mS cm^{-1} during the same period. Although there might be water chemistry effects on the overland flow and soil erosion, as a comparative study, minor variation in tap water chemistry will have no detectable influences on our result.

According to the statistics of maximum rainfall intensities for different reoccurrence periods from a multi-year rainfall regime in the soil sampling region, three constant rainfall intensities of 30, 60, and 90 mm h^{-1} (referred to hereafter as light (RI30), moderate (RI60), and extremely high (RI90)) representing 5, 50, and 100 years return period, respectively, were apllied for simulation study. All the simulated rainfalls lasted for 60 min after the initiation of overland flow.

To compare the vegetation effects on the overland flow and sediment yield, we designed expriment plots to achieve different vegetation composition and coverage. The targeted plots include: (1) control plots without vegetation (C0), (2) 50% vegetation coverage by shrub (C_S50) only and grass (C_G50) only plots, (3) 25% ($C_{S\text{-}G}25$), 50% ($C_{S\text{-}G}50$), 75% ($C_{S\text{-}G}75$), and 100% ($C_{S\text{-}G}100$) vegetation coverage by mixed shrub and grass plots. Each of all such plots has three replications installed within the effective rainfall area under each of three different rainfall intensities (Table S1).

2.2. Preparation of soil boxes and vegetation planting

2.2.1. Soil collection and soil boxes preparation

Soil was collected from the top layer (30 cm) and transported to the rainfall simulation hall from Taizicheng watershed (Longitude and latitude: 40°54′N, 115°29′E; altitude: 1700 m a.s.l.) located in the Chongli District, Zhangjiakou City, Hebei Province, China. Situated in the transition zone between the Inner Mongolia Plateau and the North China Plain, the region is controlled by a semi-arid temperate continental monsoon climate. The annual average temperature is 5.3 °C, the mean annual precipitation is 400 mm. Over 80% of the annual precipitation occurs between June and September in short-duration, high-intensity summer thunderstorms. The typical soil type on the hillslopes in the watershed is Eutric Cambisols soil (IUSS Working Group WRB, 2015), while soil depth is approximately 20–30 cm. The average soil bulk density is 1.15 g cm^{-3} (Table S2).

Soil boxes with net dimensions of 2.00 m (*L*, length) × 0.50 m (*W*, width) × 0.40 m (*D*, depth) were manufactured following the suggestions of $L \times W \times D =$ (1.00–2.00 m) × (0.50–1.00 m) × (0.22–0.50 m) (Adekalu et al., 2007; Vahabi and Nikkami, 2008). We set the soil box slope to 15° for all experiments to avoid the slope effects on the overland flow and sediment yield. An overland flow collector was installed on the soil box outlet and the sediment and overland flow samples collected during the rainfall simulation (Fig. 1a and b). In addition, evenly distributed drainage holes (1 cm aperture, 240 holes) were designed at the bottom of each soil box to allow vertical soil water movement during and after the rainfall simulations.

We filled the lowest 10 cm of soil box with sands to allow free drainage of excess water and spread a highly permeable clothes on the sand surface to separate the sand layer from the soil layer. We then filled our experimental soil into the boxes and compacted it to a bulk density of 1.15 g cm^{-3}. To achieve uniform compaction, we filled the soil into the boxes in three layers of 10 cm. We raked each soil layer lightly before adding the next level to minimize the discontinuities between layers.

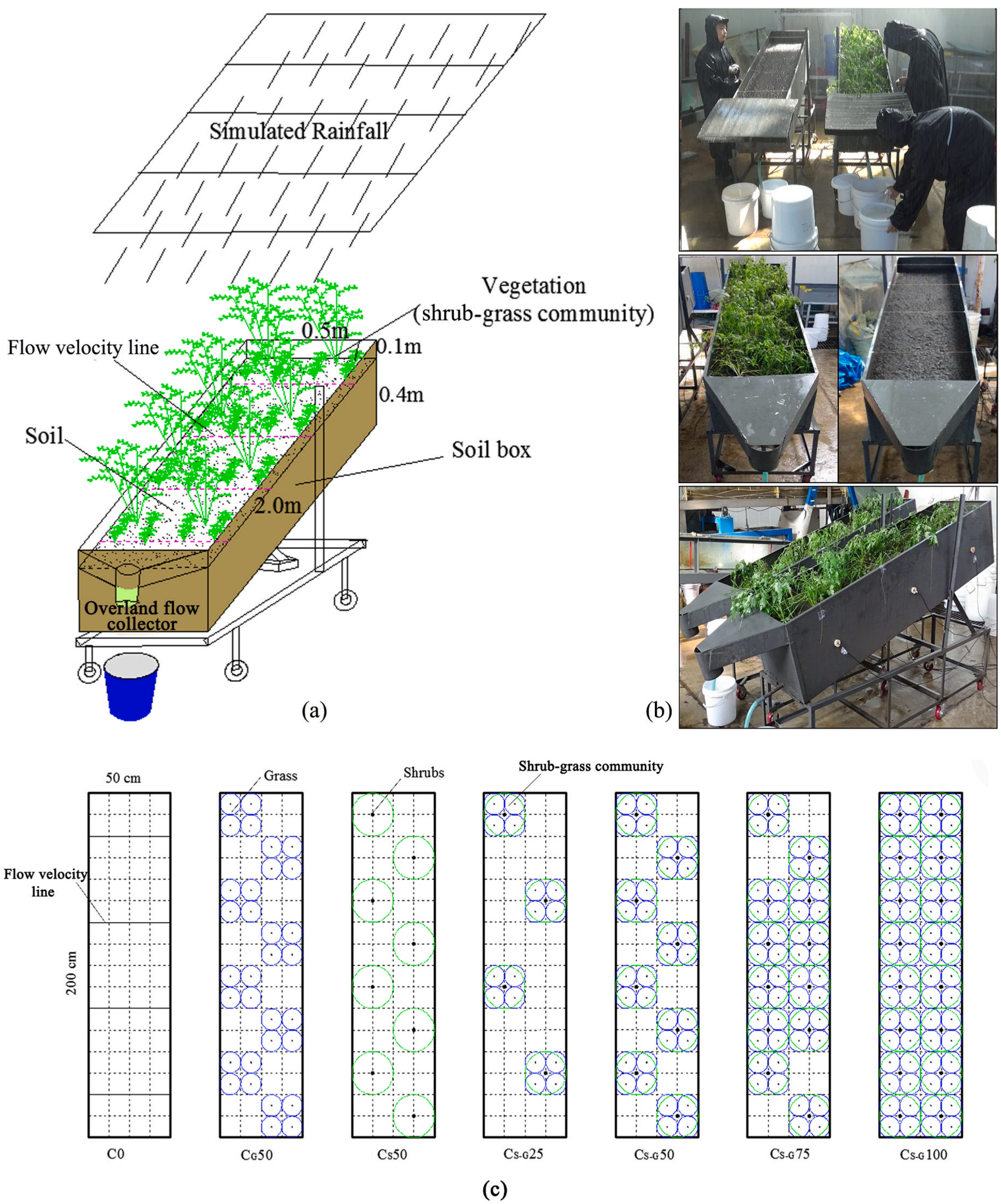

Fig. 1. Schematic diagram of simulated rainfall and soil box design (covered by vegetation) (a), photographs of boxes with and without vegetation during the rainfall simulation runs (b) and schematic diagram of vegetation coverages in the experiment (c).

The total depth of soil in the boxes was set to 30 cm.

2.2.2. Vegetation establishment

Two widely distributed indigenous species in the soil sampling region, *Lespedeza bicolor* (shrub species) and *Carex giraldiana* (grass species) were used (Xu et al., 2006a; Zhang et al., 2017b) to achieve the above-mentioned vegetative plots by using uniform planting approach. One-year-old saplings of the shrub species *Lespedeza bicolor* (approximately 50 cm in height, 25 cm × 25 cm in the crown width, 10 ± 0.50 mm in base diameter) and the grass species *Carex giraldiana* (approximately 10 cm in height, 15 cm × 15 cm in the crown width) was planted in the plots (Fig. 1).

Soil box (size 50 cm × 200 cm) was evenly divided into 64 cells (12.5 cm × 12.5 cm each cell). One grass can be planted in one cell and one shrub can be planted in four cells. And four grasses and one shrub formed a shrub-grass community (canopy coverage ratio of shrub: grass is 0.785), and the spacing of grass was 12.5 cm, the shrub was planted in the middle of four grasses (Fig. 1c). For grass only plots, 8 clusters of grass (a cluster of 4 grasses with a square shape) were planted on the soil box by diagonal uniform planting in the C_G50 plot, and the spacing of grass was 12.5 cm. For shrub only, eight shrubs were planted on the soil box by diagonal uniform planting in the C_S50 plot. For shrub-grass community, 4, 8, 12 and 16 shrub-grass communities were planted on the soil box by uniform planting in the $C_{S\text{-}G}25$, $C_{S\text{-}G}50$, $C_{S\text{-}G}75$, $C_{S\text{-}G}100$ plots, respectively (Fig. 1c). To achieve close contact between the plant roots and the soil, the vegetation was planted in May 2018. The rainfall simulation experiment was performed from July to August 2018 after two months of plant establishment. To minimize the errors to achieve the targeted vegetation coverages before the rainfall simulations, digital camera with 20 megapixel was used to obtain the photos perpendicular to the ground level and Photoshop CS 6.0 software used to calculate and identify the extra canopies for trimming.

2.3. Measurements of overland flow and sediment

We applied a RI30 pre-rainfall for around 25 min until overland flow was visible to ensure comparative uniformity of the surface soil moisture and roughness condition. A plastic sheet cover was used to prevent soil moisture evaporation and allow the soil water to equilibrate with depth for 24 h.

For each simulation run, time to overland flow initiation was recorded, experimental time then lasted for 60 min after the beginning of the overland flow. We collected overland flow and sediment samples into a bucket at intervals of 2 min in the first 10 min and 5 min later and then weighed after oven-drying at 105 °C for 24 h. Overland flow volume was measured volumetrically.

We measured overland flow velocity (Vs) at three slope sections (0.25, 0.75, and 1.25 m of slope length) at 5-min intervals. Vs was measured using $KMnO_4$ as a dye tracer and measured the travel time of the color front. We defined the upper slope from top to middle (1.75–1.25 m), the middle slope from 1.25 m to 0.75 m, and the lower slope from 0.75 to 0.25 m.

Rainfall interception and evaporation of shrub-grass canopy were negligible during the rainfall period; the infiltration rate f(t) of the slope was estimated by:

$$f(t) = Pi \times \cos\alpha - \frac{10Q_t}{(t_{i+1} - t_{i})\times S} \quad t \geq t_p \tag{1}$$

where $f(t)$ is infiltration rate at t time (mm•min^{-1}); Pi is precipitation intensity (mm•min^{-1}); α is the surface slope (°); Q_t is the corresponding discharge of each period (ml); t_i, t_{i+1} are the beginning and ending time (min); t_p is overland flow generation time (min); and S is the plot area (cm^2).

2.4. Hydrodynamic parameters calculation

We estimated the mean overland flow velocity (V, cm·s^{-1}) by:

$$V = k\, Vs \tag{2}$$

where Vs is overland flow velocity (cm·s^{-1}), and k is a coefficient equaling to 0.67 for laminar flow, 0.7 for transition flow, and 0.8 for turbulence flow (Li et al., 1996).

The flow depth (h) was calculated as:

$$h = \frac{Q}{VBt_0} \tag{3}$$

where Q is the total overland flow volume during t_0 (ml); B is the width of the overland flow section (cm); t_0 is the duration of collecting a sample of the overland flow (min).

Reynolds number (Re) and the Froude number (Fr) were used to reflect the flow regime and calculated as:

$$Re = \frac{VR}{v} \tag{4}$$

$$Fr = \frac{V}{\sqrt{gR}} \tag{5}$$

where v is kinematic viscosity (cm^2·s^{-1}) determined at the test temperature (t) by $v = \frac{0.01775}{1+0.0337t+0.000221t^2}$; R is the hydraulic radius (cm), which is approximately equal to h; g = 980 cm s^{-2}.

The Darcy-Weisbach friction coefficient (f) characterizing the flow retardation was calculated following Abrahams et al. (1986):

$$f = \frac{8gRJ}{V^2} \tag{6}$$

where J is the surface slope (m·m^{-1}) calculated as the tangent of the slope degree.

Shear stress (τ, Pa) was calculated according to Foster et al. (1984):

$$\tau = \gamma RJ \tag{7}$$

where γ is the specific gravity of water (N·m^{-3}).

Stream power (w, N·m^{-1} s^{-1}) was calculated as:

$$w = \tau V \tag{8}$$

Unit stream power (P, m·s^{-1}) was calculated as:

$$P = VJ \tag{9}$$

Unit energy of cross-section (E, cm) was the sum of water potential energy and kinetic energy and calculated according to Zhang et al. (2015):

$$E = \frac{aV^2}{2g} + h \tag{10}$$

where h is flow depth (cm); a is the correction coefficient for kinetic energy, equal to 1.

2.5. Statistical analysis

We conducted Repeated-Measures ANOVA to identify significant differences between the different treatments. The statistical analysis was performed at a significance level of 0.05 using the statistical software SPSS (IBM SPSS Statistics, 19.0).

3. Results

3.1. Overland flow

3.1.1. Overland flow against vegetation type and coverage

The shrub-grass communities were more effective to delay the overland flow generation and increase the soil infiltration than shrub only or grass only plots under the same coverage and rainfall intensity. Time to flow of the $C_{S\text{-}G}50$ plots (87.53–677.33 s) were higher than these of the C_G50 (79.85–645.70 s) and C_S50 plots (75.99–592.60 s), that was significant under rainfall intensities of RI60 and RI90 ($p < 0.05$, Table 1). And the infiltration rate (0.29–0.46 mm min^{-1}) of the $C_{S\text{-}G}50$ plots were also higher than the C_G50 (0.28–0.42 mm min^{-1}) and C_S50 plots (0.26–0.39 mm min^{-1}) while the latter was higher than the $C_{S\text{-}G}25$ plots (0.16–0.24 mm min^{-1}) (Fig. S1).

For shrub-grass communities, time to flow was significantly longer from higher coverage plots (e.g., $C_{S\text{-}G}75$ and $C_{S\text{-}G}100$) than the plot covered by $C_{S\text{-}G}25$ ($p < 0.05$), and overland flow rate and coefficient were significantly lower from higher coverage plots (e.g., $C_{S\text{-}G}75$ and $C_{S\text{-}G}100$) than the plots covered by $C_{S\text{-}G}50$ and $C_{S\text{-}G}25$ ($p < 0.05$, Table 1). The overland flow rate and overland flow coefficient decreased while the infiltration rate increased against the increase in coverage under the same rainfall intensity (Table 1, Fig. S1). The steady-state overland flow rate was reached at approximately 0.33, 0.28, 0.24, and 0.18 mm min^{-1} for the $C_{S\text{-}G}25$, $C_{S\text{-}G}50$, $C_{S\text{-}G}75$, and $C_{S\text{-}G}100$ plots, respectively, under RI30 (Fig. 2a), being reduced by 13%, 26%, 37%, and 53%, respectively, compared with the overland flow rate of 0.38 mm min^{-1} from the C0 plot. The initial and steady-state infiltration rates of the $C_{S\text{-}G}25$, $C_{S\text{-}G}50$, $C_{S\text{-}G}75$, and $C_{S\text{-}G}100$ plots were higher than that of the C0 plot (Fig. S1). The steady-state infiltration rate of 0.16, 0.20, 0.23 and 0.31 mm min^{-1} for the $C_{S\text{-}G}25$, $C_{S\text{-}G}50$, $C_{S\text{-}G}75$, and $C_{S\text{-}G}100$ plots were 45%, 82%, 109% and 182% higher than that of the C0 plot being 0.11 mm min^{-1}, respectively, under RI30 (Fig. S1a). Similar trends were observed under RI60 and RI90: 1) overland flow rate from the $C_{S\text{-}G}100$ plot leveled off at 0.42 and 0.92 mm min^{-1}, respectively (Fig. 2b and c), resulting in 55% and 32% reduction compared with that from the C0 plot that was finally stabilized at 0.94 and 1.36 mm min^{-1}, respectively; 2) the infiltration rate from the $C_{S\text{-}G}100$ plot leveled off at 0.55 and 0.54 mm min^{-1}, while the C0 plot was 0.02 mm min^{-1} and 0.09 mm min^{-1}, respectively (Fig. S1b, c). Achievement of saturated soil moisture and steady-state infiltration by progressive rainfall under a particular rainfall intensity have formed a more steady-state overland flow. There was a significant linear decrease of the overland flow rate against the shrub-grass coverages ($p < 0.05$, Fig. S2).

3.1.2. Overland flow against rainfall intensity

Overland flow rate from plots with the same vegetation coverage increased while the time to reach the relative constant infiltration rate decreased against the increase in rainfall intensity ($p < 0.05$, Fig. 2, Fig. S1 and Table 1). Overland flow rate from non-vegetated slopes (C0) reached steady-state under rainfall intensities of RI30, RI60, and RI90 at approximately 0.38, 0.94, and 1.36 mm min^{-1}, respectively (Fig. 2), indicating a significant rainfall intensity effects on the overland flow production. Similar trends were observed for plots with different vegetation coverages. Time to overland flow generation was significantly reduced against the rainfall intensity ($p < 0.05$) up to 85% reduction under RI90 compared with RI30. The overland flow coefficient increased against rainfall intensity under the same vegetation coverage (Table 1), and the infiltration coefficient decreased by 37%–65% under RI90 compared with RI30 (Fig. S1).

Average overland flow rate under RI30 decreased by 16%, 30%, 44%, and 50% from the plots covered by $C_{S\text{-}G}25$, $C_{S\text{-}G}50$, $C_{S\text{-}G}75$, and $C_{S\text{-}G}100$ compared with non-vegetated slope (C0), respectively; correspondingly, it decreased by 9%, 20%, 28%, and 34% under RI90. However, the overland flow rate under RI60 decreased more dramatically than that under RI30 and RI90 by up to 25%, 34%, 48% and 58%, respectively (Table 1). Clearly, vegetation could still reduce the overland flow volume under extreme rainfall condition (RI90).

3.2. Sediment yield

3.2.1. Sediment yield against vegetation type and coverage

Sediment yield from the $C_{S\text{-}G}50$ plots (0.13–6.73 g $min^{-1}\cdot m^{-2}$) were lower than that of the C_G50 (0.18–8.14 g $min^{-1}\cdot m^{-2}$) and C_S50 plots (0.38–9.44 g $min^{-1}\cdot m^{-2}$), that was significant under rainfall intensities of RI60 and RI90 ($p < 0.05$, Fig. 3, Table 2), indicating that shrub-grass communities had better sediment reduction benefits than shrub only or grass only treatments while the grass only were better than shrub only

Table 1
Overland flow response to vegetation coverage under three different rainfall intensities.

Overland flow parameters	Coverage	Rainfall intensity = 30 mm h^{-1} (RI30)		Rainfall intensity = 60 mm h^{-1} (RI60)		Rainfall intensity = 90 mm h^{-1} (RI90)	
		N	Mean ± Std.D	N	Mean ± Std.D	N	Mean ± Std.D
Time to flow(s)	$C_{S\text{-}G}0$	3	411.67 ± 56.19 aA	3	78.74 ± 3.07 aB	3	62.22 ± 15.19 aB
	$C_{S\text{-}G}25$	3	568.67 ± 26.63bA	3	102.10 ± 7.68bB	3	69.58 ± 13.02 aC
	C_S50	3	592.60 ± 23.70bcA	3	114.92 ± 4.60 cB	3	75.99 ± 3.04abC
	C_G50	3	645.70 ± 25.83bcA	3	126.78 ± 5.07 dB	3	79.85 ± 3.19bC
	$C_{S\text{-}G}50$	3	677.33 ± 37.54 cA	3	138.21 ± 6.75eB	3	87.53 ± 2.67 cC
	$C_{S\text{-}G}75$	3	746.33 ± 44.61cdA	3	241.42 ± 37.92 fB	3	90.81 ± 1.64 cC
	$C_{S\text{-}G}100$	3	930.00 ± 122.16eA	3	289.44 ± 34.67gB	3	95.46 ± 4.91 cC
Overland flow rate (mm•min^{-1})	$C_{S\text{-}G}0$	3	0.31 ± 0.02 aA	3	0.86 ± 0.05 aB	3	1.30 ± 0.07 aC
	$C_{S\text{-}G}25$	3	0.26 ± 0.03bA	3	0.65 ± 0.03bB	3	1.18 ± 0.06bC
	C_S50	3	0.24 ± 0.01bcA	3	0.62 ± 0.03bcB	3	1.12 ± 0.06bcC
	C_G50	3	0.22 ± 0.01 cA	3	0.59 ± 0.03 cB	3	1.08 ± 0.05bcC
	$C_{S\text{-}G}50$	3	0.22 ± 0.02 cA	3	0.56 ± 0.03 dB	3	1.04 ± 0.05 cC
	$C_{S\text{-}G}75$	3	0.17 ± 0.01 dA	3	0.44 ± 0.02eB	3	0.94 ± 0.04 dC
	$C_{S\text{-}G}100$	3	0.15 ± 0.02eA	3	0.36 ± 0.02 fB	3	0.85 ± 0.03 dC
Overland flow coefficient	$C_{S\text{-}G}0$	3	0.62 ± 0.04 aA	3	0.86 ± 0.05 aB	3	0.87 ± 0.05 aB
	$C_{S\text{-}G}25$	3	0.52 ± 0.05bA	3	0.65 ± 0.03bB	3	0.78 ± 0.04bC
	C_S50	3	0.49 ± 0.02bcA	3	0.62 ± 0.03bcB	3	0.75 ± 0.04bcC
	C_G50	3	0.45 ± 0.02 cA	3	0.59 ± 0.03 cB	3	0.72 ± 0.04bcC
	$C_{S\text{-}G}50$	3	0.43 ± 0.04 cA	3	0.56 ± 0.03 dB	3	0.69 ± 0.04 cC
	$C_{S\text{-}G}75$	3	0.35 ± 0.03 dA	3	0.45 ± 0.02eB	3	0.62 ± 0.03 dC
	$C_{S\text{-}G}100$	3	0.31 ± 0.04eA	3	0.36 ± 0.02 fA	3	0.57 ± 0.02 dB

Note: Different capital letters in the same row mean the significant difference between different rainfall intensities (ANOVA, $p < 0.05$); Different lowercase letters in the same column mean the significant difference between different vegetation coverages (ANOVA, $p < 0.05$).

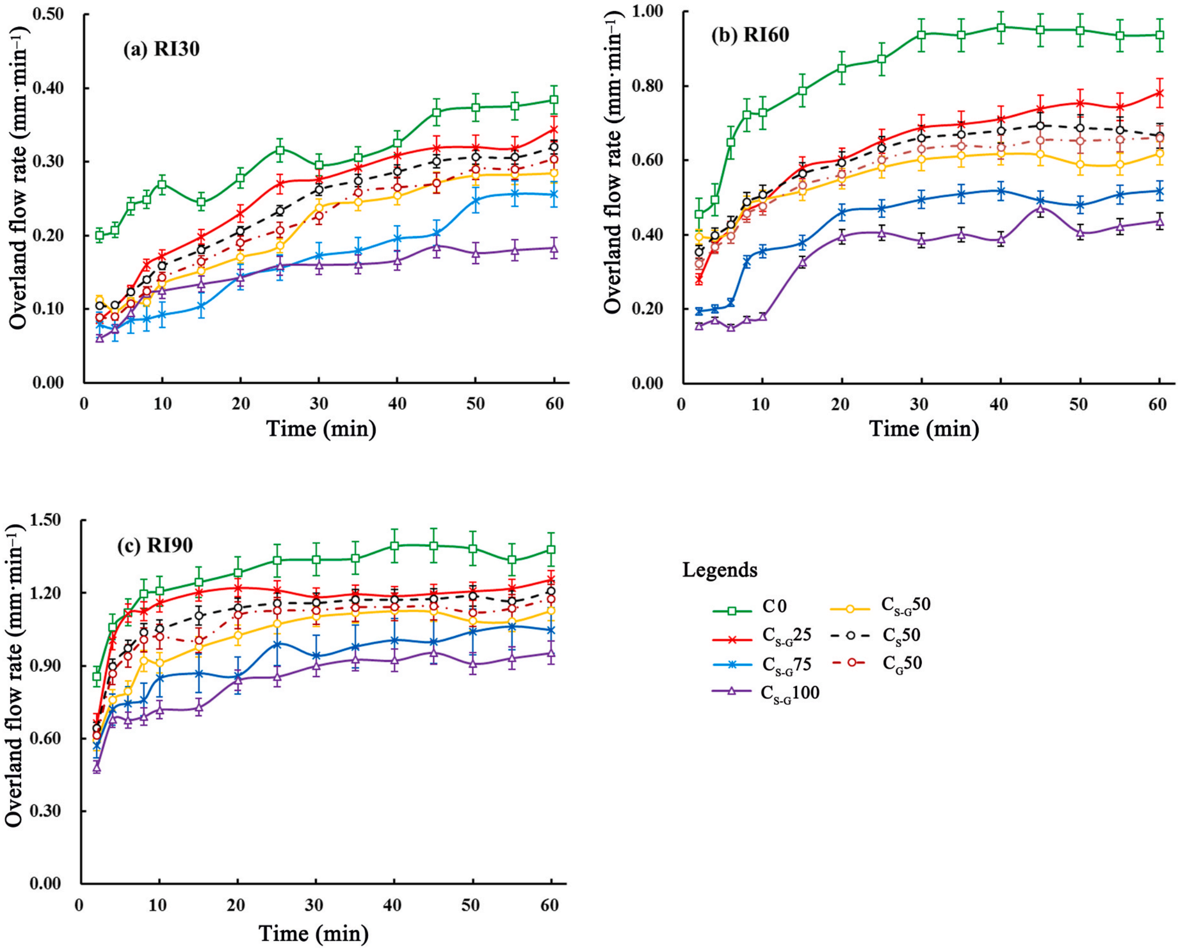

Fig. 2. Overland flow hydrograph for different vegetation coverages under three rainfall intensities of RI30 (a), RI60 (b), and RI90 (c), respectively. Error bars are standard deviations.

treatments.

For shrub-grass communities, mean sediment yield showed a decreasing trend against vegetation coverage increase under the same rainfall intensity (Fig. 4). Under RI30, the mean sediment yield of the C0 plot was 1.21 g $min^{-1}·m^{-2}$, which is much higher than that from the vegetated slopes with 0.65, 0.13, 0.04, and 0.02 g $min^{-1}·m^{-2}$ for $C_{S\text{-}G}25$, $C_{S\text{-}G}50$, $C_{S\text{-}G}75$, and $C_{S\text{-}G}100$ plots, respectively (Table 2). The maximum reduction in sediment yield was 1.19 g $min^{-1}·m^{-2}$ (approximately 98%) from the $C_{S\text{-}G}100$ plot under RI30 compared to the C0 plot. For RI60 and RI90, the mean sediment yield of the $C_{S\text{-}G}100$ plot was 1.32 and 4.03 g $min^{-1}·m^{-2}$, compared to the C0 plots with 10.45 and 15.22 g $min^{-1}·m^{-2}$, respectively. The $C_{S\text{-}G}100$ plot thus could reduce the sediment yield by 87% and 73%, respectively (Table 2). The benefit of vegetation on sediment reduction decreased with the increase of rainfall intensity.

The ANOVA analysis showed that the mean sediment yield under coverages of $C_{S\text{-}G}50$, $C_{S\text{-}G}75$, and $C_{S\text{-}G}100$ were significantly lower than for coverages of $C_{S\text{-}G}25$ and C0 ($p < 0.05$, Table 2, Fig. 3, Fig. 4). Similar to overland flow generation, the mean sediment yield was significantly correlated with the vegetation coverage in a negative way under the same rainfall intensities. In addition, the mean sediment yield exponentially decreased against the increase in vegetation coverage for the shrub-grass coverage ($R^2 = 0.97$, $p < 0.05$ for RI30, $R^2 = 0.98$, $p < 0.05$ for RI60 and $R^2 = 0.94$, $p < 0.05$ for RI90, Fig. 4).

3.2.2. *Sediment yield against rainfall intensity*

Sediment yield from plots with the same vegetation coverage increased significantly against the increase in rainfall intensity ($p < 0.05$, Fig. 3, Table 2). For RI30 and RI60, the sediment yield increased rapidly at the initial stage of the experiments and declined after reaching a peak at approximately 10 min (Fig. 3), almost concurrent with peak overland flow (Fig. 2). However, for RI90, the sediment yield peaked at the very beginning and declined gradually afterwards. For the C0 plots, the constant sediment yield for RI60 and RI90 were 10.44 and 13.05 g $min^{-1}·m^{-2}$ (Fig. 3), 13 and 16 times greater compared with 0.76 g $min^{-1}·m^{-2}$ for RI30, respectively. For the plots with $C_{S\text{-}G}50$, the constant sediment yield under RI30, RI60, and RI90 were 0.10, 3.38, and 5.78 g $min^{-1}·m^{-2}$, respectively (Fig. 3) and sediment yield under RI60 and RI90 increased by 33 and 57 times compared with that under RI30, respectively. For the plots with other coverages, the sediment yield showed a similar trend under different rainfall intensities. In addition, there were no significant difference in sediment yield under RI30 between the plots covered by vegetation over 50% while a significant difference was observed between plots with different coverages under RI60 and RI90 (Table 2).

3.3. *Hydrodynamic characteristics*

3.3.1. *Vegetation type, coverage and overland flow hydrodynamic characteristics*

Mean overland flow velocity (1.91, 3.93, 4.98 cm s^{-1} under rainfall intensity of RI30, RI60 and RI90, respectively) over $C_{S\text{-}G}50$ plots were lower than that of the C_G50 (2.73, 4.34, 5.30 cm s^{-1}) and C_S50 plots (3.25, 5.46, 6.66 cm s^{-1}) (Table 3, Fig. S3). The Darcy-Weisbach friction coefficient (*f*) of the $C_{S\text{-}G}50$ plots were 1.15–2.80 times and 2.20–4.34

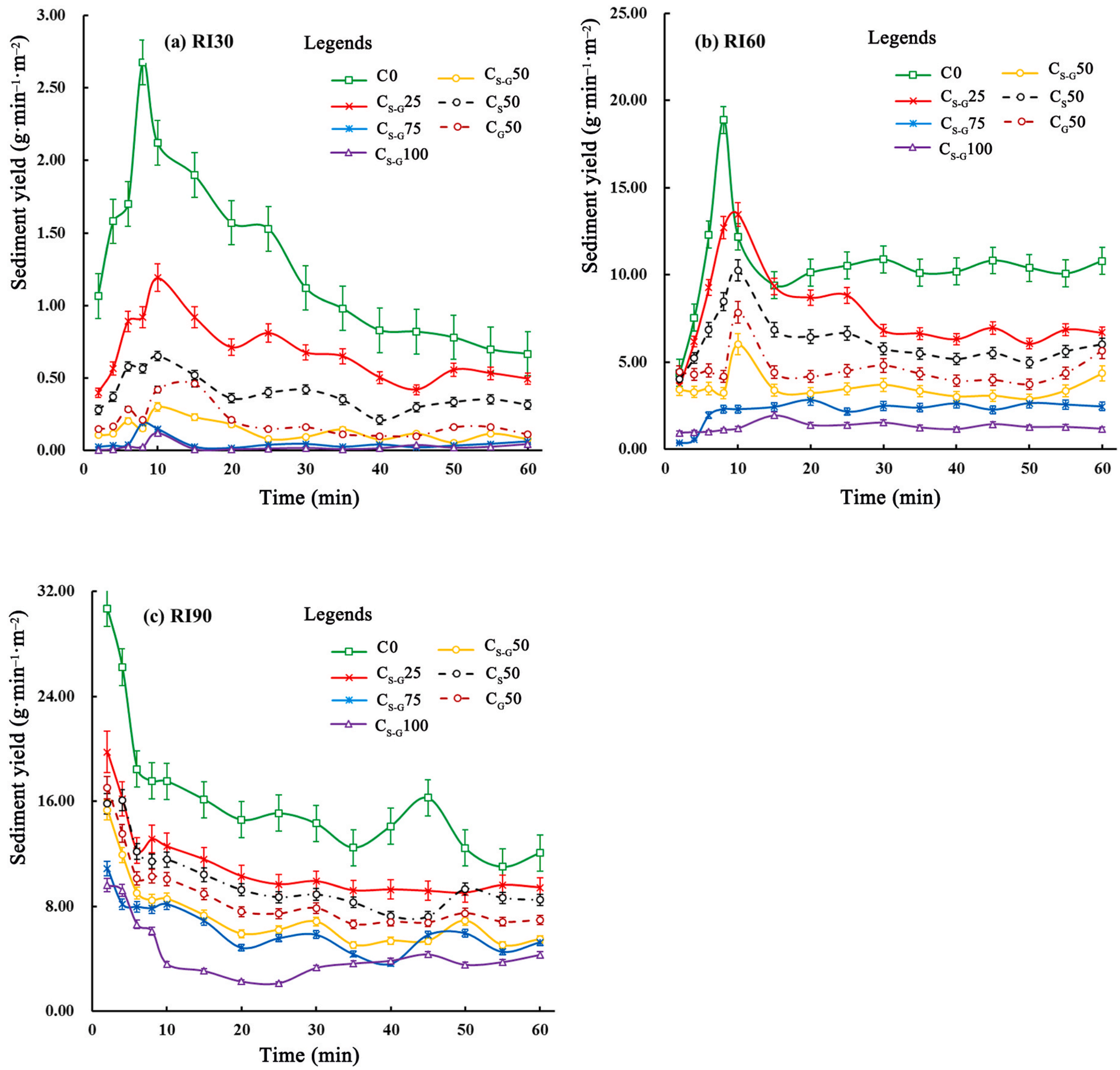

Fig. 3. Sediment hydrograph for different vegetation coverages under three rainfall intensities of RI30 (a), RI60 (b), and RI90 (c), respectively. Error bars are standard deviations.

Table 2
Sediment response with different rainfall intensities and vegetation coverages (unit: g•min^{-1}•m^{-2}).

Coverage	Rainfall intensity = 30 mm h^{-1}		Rainfall intensity = 60 mm h^{-1}		Rainfall intensity = 90 mm h^{-1}	
	N	Mean ± Std.D	N	Mean ± Std.D	N	Mean ± Std.D
C0	3	1.21 ± 0.10 aA	3	10.45 ± 0.50 aB	3	15.22 ± 0.60 aC
$C_{S\text{-}G}25$	3	0.65 ± 0.20 aA	3	7.61 ± 0.40bB	3	12.23 ± 0.50bC
C_S50	3	0.38 ± 0.02 cA	3	6.03 ± 0.30 cB	3	9.44 ± 0.47 cC
C_G50	3	0.18 ± 0.01bA	3	4.50 ± 0.23 dB	3	8.14 ± 0.41 cC
$C_{S\text{-}G}50$	3	0.13 ± 0.02bA	3	3.46 ± 0.20eB	3	6.73 ± 0.30 dC
$C_{S\text{-}G}75$	3	0.04 ± 0.01 dA	3	2.32 ± 0.30 fB	3	5.82 ± 0.30eC
$C_{S\text{-}G}100$	3	0.02 ± 0.00 dA	3	1.32 ± 0.20gB	3	4.03 ± 0.03 fC

Note: Different capital letters in the same row mean the significant difference between different rainfall intensities (ANOVA, $p < 0.05$); Different lowercase letters in the same column mean the significant difference between different vegetation coverages (ANOVA, $p < 0.05$).

times greater than that from C_G50 and C_S50 plots, respectively. Laminar flow ($Re < 500$) and slow flow ($Fr < 1$) on the $C_{S\text{-}G}50$, C_G50 and C_S50 plots were formed under all rainfall intensities. The $C_{S\text{-}G}50$ plots had lower stream power (ω, P) and higher shear stress (τ) and flow depth (h) than the C_G50 and C_S50 plots (Table 3). It showed that shrub-grass communities were more effective to increase the flow resistance and flow depth, reduce overland flow velocity and stream power than shrub only or grass only plots under the same coverage and rainfall intensity.

For shrub-grass communities, overland flow velocity increased as the rainfall progressed while decreased against the increase in coverage (Fig. S3). Mean overland flow velocity (V) of 6.35 cm s^{-1} from the non-vegetated slope (C0) was approximately 2–3 times of that from shrub-grass plots $C_{S\text{-}G}50$ (3.93 cm s^{-1}) and $C_{S\text{-}G}100$ (2.42 cm s^{-1}) under RI 60, respectively; while the mean flow velocity from slopes of the $C_{S\text{-}G}25$, $C_{S\text{-}G}50$, $C_{S\text{-}G}75$, and $C_{S\text{-}G}100$ plots were lowered by 25%, 38%, 52%, and 62%, respectively, compared to C0 (Table 3). Under RI30 and RI90, the flow velocity of $C_{S\text{-}G}100$ decreased by 71% and 55% compared with the flow velocity of the C0 plot, respectively. A similar trend in the mean h, ranging from 0.45 mm to 0.50 mm when the vegetation coverage increased under RI60. The increase of vegetation coverage correspondingly enhanced the overland flow resistance. The f changed from

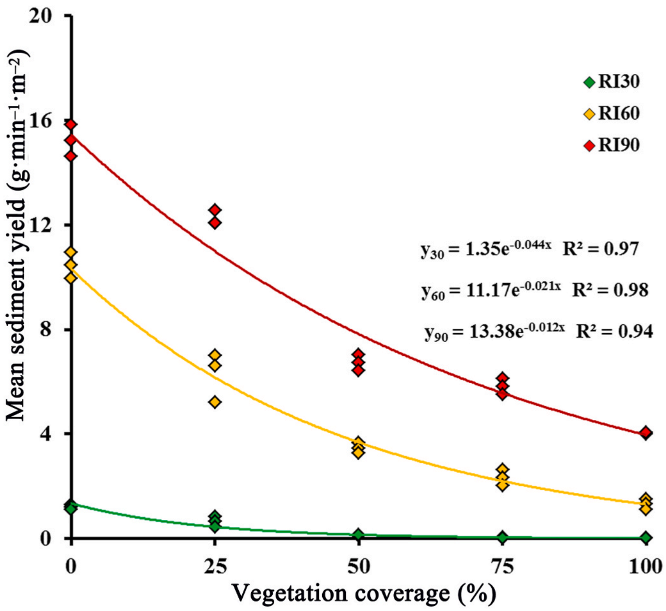

Fig. 4. Relationships between the mean sediment yield and vegetation coverage under rainfall intensity of RI30, RI60 and RI90, respectively.

17.39 ($C_{S\text{-}G}100$) to 2.27 (C0), which corresponds to an eightfold change (Table 3). There was no obvious rill development and turbulent conditions (*Re* < 500) on all slopes (Table 3). However, a considerable irregular flow pattern ($Fr = 0.95$) was observed under RI60 and slower overland flow velocities on all slopes covered with vegetation (Table 3). The increase in vegetation coverage led to the reduction in ω, P and the increase in τ under the same rainfall intensity. For instance, under RI60, the τ increased from 1.146 on the C0 plot to 1.272 on the $C_{S\text{-}G}100$ plot, the P decreased from 0.016 to 0.006 and the ω declined by 58%. Flow depth increase due to the increasing vegetation coverage could lead to the increase in τ. The E was reduced with increasing vegetation coverage under RI60, while there were no significant change trend between E and vegetation coverage increase under both RI30 and RI90 (Table 3).

3.3.2. Rainfall intensity and overland flow hydrodynamic characteristics

The V, Re and Fr were all increased against the increase in rainfall intensity (Table 3). The mean overland flow velocity on the $C_{S\text{-}G}100$ plots under RI30, RI60, and RI90 was reduced by 71%, 62%, and 55% compared to the C0 plot, respectively. The Re of all plots with different coverages was between 5.24 and 49.78 for different rainfall intensities, indicating that all flows were laminar. Fr of all plots with different coverages was between 0.193 and 0.982 (<1.0), suggesting that all flows were slow.

For the same coverage, the f decreased with the increase of rainfall intensity. The f of the $C_{S\text{-}G}100$, $C_{S\text{-}G}75$, $C_{S\text{-}G}50$ plots under RI90 were only 20%–30% of that under RI30, indicating that the vegetation effect on flow resistance was smaller in the case of heavy rainfall (Table 3). Table 3 also shows that the τ, E, ω, and P increased with increasing rainfall intensities. Meanwhile, the overland flow pattern on the plot surface was in an unsteady state, and the variation range was also increasing with the increase of rainfall intensity.

3.3.3. Overland flow hydrodynamics and soil erosion

Mean sediment yield showed an increasing trend against shear stress (τ) under different shrub-grassland coverages (Fig. 5a, Table 3), which indicated that the soil erodibility increased with the increase of τ. The critical shear stress (τ_0) of the $C_{S\text{-}G}100$, $C_{S\text{-}G}75$, $C_{S\text{-}G}50$, $C_{S\text{-}G}25$ and C0 plots were 0.97, 0.94, 0.86, 0.57 and 0.52 N m^{-2}, respectively, indicating that the τ_0 of vegetation covered plots was higher than that of bare plots and increased with increasing shrub-grass coverage. The sediment yield increased with the increase of ω and P (Fig. 5b and c). The increasing shrub-grassland coverage reduced the sediment yield and the stream power (Table 2, Table 3). The critical stream power (ω_0) of the C0, $C_{S\text{-}G}25$, $C_{S\text{-}G}50$, $C_{S\text{-}G}75$ and $C_{S\text{-}G}100$ plots were 0.016, 0.016, 0.015, 0.013 and 0.012 N m^{-1}•s^{-1}, and the critical unit stream power (P_0) were 0.010, 0.009, 0.005, 0.004 and 0.003 m s^{-1}, respectively. From the energy point of view, the critical overland flow energy of soil erosion was different under different vegetation coverage, which increased with the increase of vegetation coverage. The critical unit energy of cross-section (E_0) of the C0, $C_{S\text{-}G}25$, $C_{S\text{-}G}50$, $C_{S\text{-}G}75$ and $C_{S\text{-}G}100$ plots were 0.028, 0.028, 0.036, 0.038 and 0.039 cm, respectively (Fig. 5d).

The ω and P on the $C_{S\text{-}G}100$ plots under RI30, RI60, and RI90 was reduced by 50%, 58%, 51%, and 73%, 63%, 53% compared to the C0

Table 3
Hydrodynamic parameters under different experiment conditions.

Rainfall intensity	Vegetation coverage	V (cm•s^{-1})	h (mm)	Re	Fr	f	E (cm)	τ (N•m^{-2})	P (m•s^{-1})	ω (N•m^{-1}•s^{-1})
RI30	C0	4.29 ± 0.38 aA	0.24	11.19	0.88	2.66	0.034	0.614	0.011	0.026
	$C_{S\text{-}G}25$	3.48 ± 0.38bA	0.25	9.07	0.70	4.20	0.031	0.635	0.009	0.022
	C_S50	3.25 ± 0.40bA	0.25	8.88	0.66	4.81	0.030	0.636	0.008	0.021
	C_G50	2.73 ± 0.34 cA	0.27	8.15	0.53	7.45	0.031	0.695	0.007	0.019
	$C_{S\text{-}G}50$	1.91 ± 0.33 dA	0.38	7.79	0.32	20.87	0.040	0.956	0.005	0.018
	$C_{S\text{-}G}75$	1.49 ± 0.16eA	0.39	6.18	0.24	35.62	0.040	0.988	0.004	0.015
	$C_{S\text{-}G}100$	1.23 ± 0.11eA	0.41	5.24	0.19	55.36	0.042	1.051	0.003	0.013
RI60	C0	6.35 ± 0.71 aB	0.45	30.47	0.95	2.27	0.066	1.146	0.016	0.073
	$C_{S\text{-}G}25$	4.75 ± 0.83bB	0.45	23.49	0.71	4.07	0.057	1.150	0.012	0.055
	C_S50	5.46 ± 0.96 cB	0.38	22.41	0.90	2.56	0.053	0.955	0.014	0.052
	C_G50	4.34 ± 0.77bdB	0.45	21.29	0.65	4.85	0.055	1.142	0.011	0.050
	$C_{S\text{-}G}50$	3.93 ± 0.72 dB	0.48	20.50	0.57	6.29	0.056	1.214	0.010	0.048
	$C_{S\text{-}G}75$	3.05 ± 0.57eB	0.49	16.35	0.44	10.62	0.053	1.236	0.008	0.038
	$C_{S\text{-}G}100$	2.42 ± 0.66 fB	0.50	13.20	0.35	17.39	0.053	1.272	0.006	0.031
RI90	C0	7.43 ± 0.75 aC	0.58	49.78	0.98	2.15	0.087	1.482	0.019	0.110
	$C_{S\text{-}G}25$	5.87 ± 0.54bC	0.67	44.75	0.73	3.94	0.084	1.697	0.015	0.100
	C_S50	6.66 ± 0.48 cC	0.56	40.87	0.90	2.57	0.079	1.428	0.017	0.095
	C_G50	5.30 ± 0.42 dC	0.68	39.42	0.65	4.93	0.083	1.731	0.014	0.092
	$C_{S\text{-}G}50$	4.98 ± 0.59 dC	0.69	37.95	0.60	5.68	0.082	1.761	0.013	0.088
	$C_{S\text{-}G}75$	4.34 ± 0.57eC	0.72	35.14	0.52	7.75	0.082	1.827	0.011	0.079
	$C_{S\text{-}G}100$	3.32 ± 0.32 fC	0.86	31.88	0.36	15.80	0.091	2.174	0.009	0.072

Note: Different capital letters in the same column mean the significant difference between different rainfall intensities (*ANOVA*, $p < 0.05$); Different lowercase letters in the same column mean the significant difference between different vegetation coverages (*ANOVA*, $p < 0.05$).

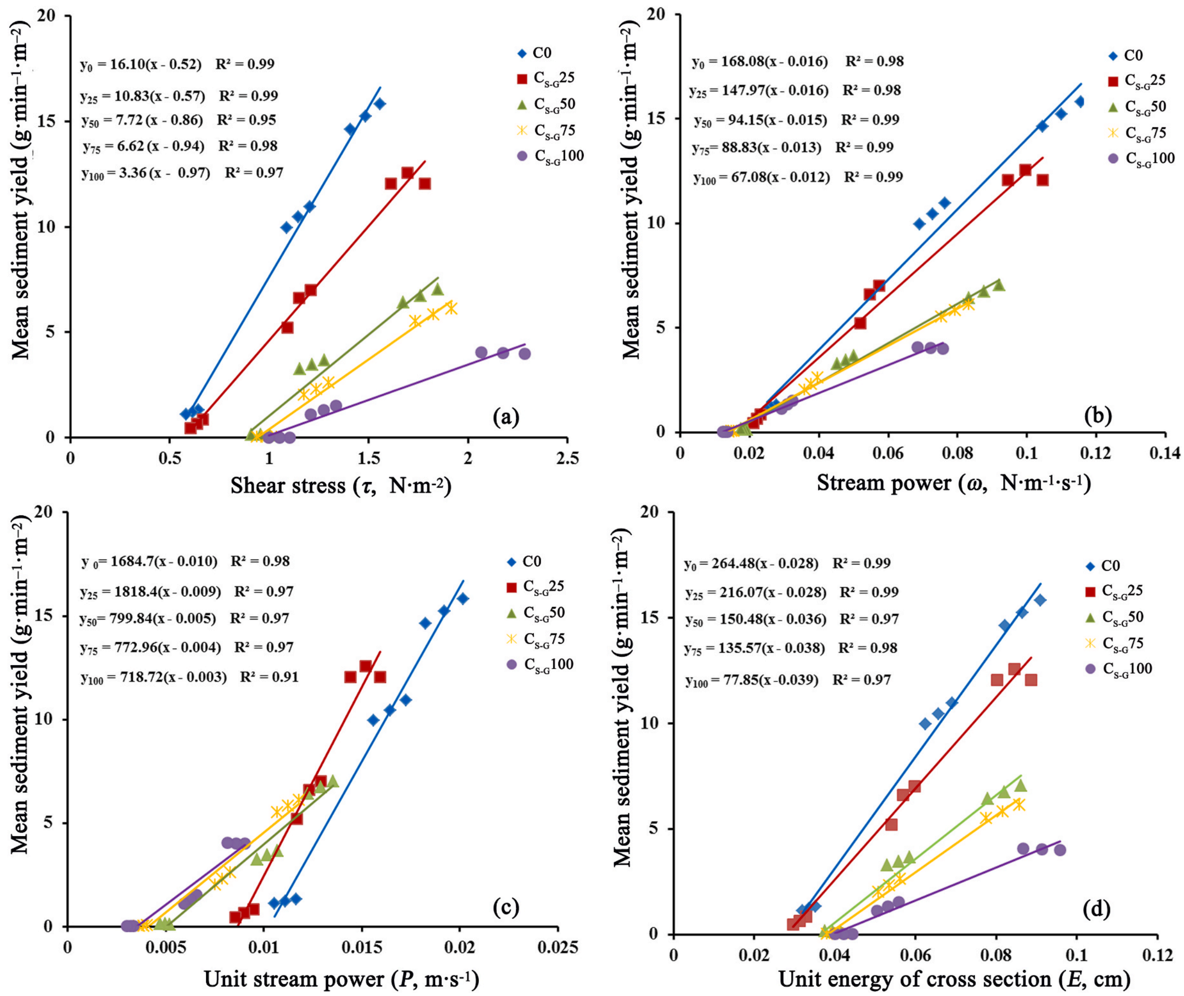

Fig. 5. The relationships between the mean sediment yield and shear stress (τ) (a), stream power *(w)* (b), unit stream power (*P*) (c) and unit energy of cross section (*E*) (d), respectively, under different vegetation coverages.

plot, respectively. At the same time, the sediment yields were reduced by 98%, 87%, and 74% from the $C_{S\text{-}G}100$ plot compared to the C0 plot under RI30, RI60, and RI90, respectively (Table 2, Table 3). Clearly, the stream power of overland flow decreased with the increase of vegetation coverage on the slope. Under extreme rainfall condition (RI90), vegetation could still reduce the overland flow power and slow down the soil erosion.

4. Discussion

4.1. Effects of vegetation type and coverage on overland flow

Vegetation posts a significant impact on the hydrological cycling by regulating soil infiltration and the overland flow (Pan et al., 2017; Qu et al., 2013; Sun et al., 2019; Zhang et al., 2014a). Four to thirteen percent reduction in overland flow from the shrub-grass community covered slopes compared with shrub only and grass only covered slopes under the same canopy coverage of 50% and such reduction from all shrub-grass slopes relative to the bare slopes ranged from 9% to 58% (Fig. 2). In contrast, the percentage increment in infiltration rate from all shrub-grass slopes relative to bare slopes were more than 45% (Fig. S1). The combined action of shrub and grass could increase surface roughness, reduce overland flow velocity, and then extend the soil infiltration time, increase the soil infiltration, and decrease the overland flow volume more significantly than shrub only and grass only hillslopes do (Table 1, Fig. 2, Fig. S1) (Almeida et al., 2018; Gu et al., 2020; Zhao et al., 2019). In addition, the grass coverage exhibits a better water retention capacity than the shrub coverage, which is consistent with previous findings (Han et al., 2021; Zhao et al., 2019).

A significant linear decrease in overland flow against the shrub-grass communities coverages under the same rainfall intensity (Fig. S2, Table 1) is consistent with previous findings for single lifeform vegetation covered slopes (Han et al., 2021; Wei et al., 2014; Xiao et al., 2011b; Zhao et al., 2019). Under all the conditions of RI30, RI60 and RI90, the Darcy-Weisbach friction coefficient (*f*) with vegetation-covered slopes were all higher than those slopes without vegetation, and the flow generally occurred faster on low coverage plots than high coverage plots (Table 1), which is consistent with previous findings (Cai et al., 2021; Chen et al., 2018; Han et al., 2021; Liu et al., 2018). In addition, the overland flow pattern and the flow velocity slowed down, the Froude number (*Fr*) decreased, and the flow resistance coefficient increased with the increase of shrub-grass communities coverage. With the increase in flow depth (*h*), the frictional resistance also increased, then the pressure difference in the vortex area behind the vegetation in the backwater area after vegetation met the water surface also increased, and the slow-flow capacity increased significantly, which lead to the extension of the time to flow and the time of flow residence (Cai et al., 2021; Zhang et al., 2021).

4.2. Effects of vegetation on the overland flow hydrodynamics and soil erosion

Vegetation type and coverage are essential factors that impact overland flow and sediment yield (Li et al., 2014; Lin et al., 2018; Zhang et al., 2014b). Compared with the shrub only and grass only covered slopes, sediment yield from mixed shrub and grass slopes was reduced by 20%–190% under the same conopy coverage of 50% (Table 2, Fig. 3) due to the increased surface roughness, reduced overland flow velocity and stream power as well as change the flow pattern (Table 3) (Han et al., 2021; Hou et al., 2014; Mohammad and Adam, 2010; Zhao et al., 2019). In addition, the mean sediment yield decreased exponentially with the increase in vegetation coverage for the shrub-grass coverage under the same rainfall intensity (Fig. 4) indicating the significant role played in controlling soil erosion by vegetation cover (Gyssels et al., 2005; Liu et al., 2014). In this study, when shrub-grass coverage rose from C0 to $C_{S\text{-}G}100$, the sediment yield decreased by 87% for RI60, meanwhile the f increased eightfold, but the E, w, P decreased by 20%, 58% and 62%, respectively (Table 2). That was because more energy from raindrops and overland flow were dissipated by overcoming the flow resistance and thus flow velocity reduced and less energy left for soil detachment and sediment transport against the increase in vegetation coverage(Palucis et al., 2018; Papanicolaou et al., 2018; Sun et al., 2019; Yang et al., 2016; Zhang et al., 2017).

Rainfall intensity is an important direct factor affecting overland flow and sediment yield (Yan et al., 2018). The sediment yield increased significantly against the increase in rainfall intensity under the same vegetation coverage (Fig. 3, Table 2). The increase of rainfall intensity made the flow pattern become more rapid, significantly increased the flow velocity, and then increased the shear stress of overland flow, stream power and overland flow energy (Fig. 3), leading to the enhanced erosion capacity of overland flow (Mahmoodabadi and Sajjadi, 2016; Wu et al., 2017; Zhao et al., 2019).

Mean sediment yield showed an increasing trend against τ, ω, P and E under different shrub-grass coverages (Fig. 5, Table 3). Meanwhile, the critical shear stress (τ_0) and overland flow energy (E_0) increased, while the critical stream power (ω_0) and unit stream power (P_0) decreased with the increase of vegetation coverage (Fig. 5). The increase in shrub-grass coverage increased surface roughness leading to the greater overland flow shear stress to reach the critical value and disperse soil particles at the early stages of rainfall events (Sirjani and Mahmoodabadi, 2014; Yu et al., 2010). Increase in the vegetation coverage increased the capacity of overland flow retention, reduced initial flow velocity and increased the overland flow depth, potential energy and critical initial flow energy (E_0) and led to the reduction in the kinetic energy and the stream power of the overland flow (Palucis et al., 2018; Papanicolaou et al., 2018; Sun et al., 2019).

4.3. Implications

Overland flow and soil erosion from hillslopes in the real world involve complicated physical processes and multiple agents especially when the slopes are covered by vegetations (Krause et al., 2017; Sun et al., 2019). Alternatively, indoor rainfall simulations provide the most knowledge for understanding hydrodynamic processes of overland flow and soil erosion under different vegetative conditions(Cao et al., 2015; Zhou et al., 2008). In addition, such experimental data are valuble for calibrating and validating soil erosion models including the Universal Soil Loss Equation (USLE), Revised USLE (RUSLE) (Dissmeyer and Foster, 1980; Zhang et al., 2011) and the Water Erosion Prediction Project (WEPP) (Dun et al., 2009; Elliot, 2004) even though such models involve also empirical equations as well. For instance, measured runoff and sediment yield from vegetated slopes can be used to calibrate and validate the vegetaton factors against the calculated soil loss by USLE/RUSLE model with fixed rainfall erosivity and slope factors. On the other hand, rainfall simulation generated hydrodynamic paramters such as flow shear stress can be directly used in phydical processes based WEPP model, unit stream power or stream power for EUROSEM, LISEM and GUEST models (Hao et al., 2017).

In addition, mixed shrub and grass communities are very effective to conserve soil and water in water-limited and highland regions. Thus, establishing shrub-grass buffer zone on sloping farmland and stream banks can be used as a bioengineering approach to control the soil erosion and prevent riverbed scouring and reduce sediment entering the river channel (Dunn et al., 2011; Sun et al., 2019). Further, such measures can also reduce the nitrogen, phosphorus and other nutrients from agricultural areas entering the river, forming a defense line to control non-point source pollution and ultimately achieve the sustainable management of watersheds with multiple land uses in dryland or highland regions (Dunn et al., 2011; Sun et al., 2019).

5. Conclusion

Understanding vegetation effects on the hillslope overland flow and soil erosion in a hydrodynamic approach is essential for developing sound soil and water conservation practices in water-limited and/or highland regions. Shrub-grass communities had better overland flow and sediment reduction benefits than shrub only and grass only covered slopes. The overland flow rate linearly decreased while the mean sediment yield exponentially reduced against the increase in vegetation coverage under simulated rainfall. Overland flow volume and sediment load from vegetated slopes were reduced by 9%–58% and 27%–98%, respectively, compared with unvegetated slopes while the infiltration rate collectively increased by over 45%. Although the overland flow under all the experiment setup was laminar, the increase in vegetation coverage of the shrub-grass community effectively increased the resistance coefficient and significantly reduce the stream power, leading to reduced overland flow and soil erosion from the vegetative slope even under extreme rainfall. The flow velocity, the shear stress of overland flow, stream power and overland flow energy increased with the increase of rainfall intensity. We highlight that establishing shrub-grass community and increasing the vegetation coverage is an effective measure to conserve soil and water in water-limited and highland regions.

Funding sources

The study was financially supported by the Major Science and Technology Program for Water Pollution Control and Treatment of China (Grant No. 2017ZX07101002-002).

Credit author statement

Ph.D. candidate Xiao Li has conducted the data analysis and drafted the manuscript; Ph.D. candidate Xiao Li and Yifan Zhang performed the experiments, collected data, and processing the data; Prof. Zhiqiang Zhang instructed all the data processing, data analysis, manuscript writing and revisions; Prof. Xiaodong Ji and Dr. Peter Strauss helped to develop the ideas, extend the discussion, and revise the manuscript.

Declaration of competing interest

The authors declare that they have no known competing financial interests or personal relationships that could have appeared to influence the work reported in this paper.

Appendix A. Supplementary data

Supplementary data to this article can be found online at https://doi.org/10.1016/j.envres.2022.113774.

References

Abrahams, A.D., Parsons, A.J., Luk, S.H., 1986. Field measurement of the velocity of overland flow using dye tracing. Earth Surf. Proc. Land 11, 653–657. https://doi.org/10.1002/esp.3290110608.

Adekalu, K.O., Olorunfemi, I.A., Osunbitan, J.A., 2007. Grass mulching effect on infiltration, surface runoff and soil loss of three agricultural soils in Nigeria. Bioresour. Technol. 98, 912–917. https://doi.org/10.1016/j.biortech.2006.02. 044.

Allton, K.E., Harris, J.A., Rickson, R.J., Ritz, K., 2007. The effect of microbial communities on soil hydrological processes: a microcosm study utilising utilizing simulated rainfall. Geoderma 142, 11–17. https://doi.org/10.1016/j.geoderma.2007.06.004.

Almeida, W., Panachuki, E., Oliveira, P., Silva, R.M.D., Menezes, R.D.S., Sobrinho, T.A., Carvalho, D.F.D., 2018. Effect of soil tillage and vegetal cover on soil water infiltration. Soil Till. Res 175, 130–138. https://doi.org/10.1016/j.still. 2017.07.009.

Arnaez, J., Lana-Renault, N., Lasanta, T., Ruiz-Flano, P., Castroviejo, J., 2015. Effects of farming terraces on hydrological and geomorphological processes, A review. Catena 128, 122–134. https://doi.org/10.1016/j.catena.2015.01.021.

Borrelli, P., Robinson, D.A., Fleischer, L.R., Lugato, E., Ballabio, C., Alewell, C., Meusburger, K., Modugno, S., Schütt, B., Ferro, V., Bagarello, V., Van Oost, K., Montanarella, L., Panagos, P., 2017. An assessment of the global impact of 21st century land use change on soil erosion. Nat. Commun. 8, 2013. https://doi.org/10.1038/s41467-017-02142-7.

Cai, Z., Wang, J., Yang, Y., Zhang, R., 2021. Influence of vegetation coverage on hydraulic characteristics of overland flow. Water 13, 1055. https://doi.org/10.3390/w13081055.

Cao, L.X., Liang, Y., Wang, Y., Lu, H.Z., 2015. Runoff and soil loss from *Pinus massoniana* forest in southern China after simulated rainfall. Catena 129, 1–8. https://doi.org/10.1016/j.catena.2015.02.009.

Cerdà, A., 2007. Soil water erosion on road embankments in eastern Spain. Sci. Total Environ. 378, 151–155. https://doi.org/10.1016/j.scitotenv.2007.01.041.

Chen, H., Zhang, X.P., Abla, M., Lü, D., Yan, R., Ren, Q.F., Ren, Z.Y., Yang, Y.H., Zhao, W.H., Lin, P.F., Liu, B.Y., Yang, X.H., 2018. Effects of vegetation and rainfall types on surface runoff and soil erosion on steep slopes on the Loess Plateau, China. Catena 170, 141–149. https://doi.org/10.1016/j.catena.2018.06.006.

Dissmeyer, G.E., Foster, G.R., 1980. A Guide for Predicting Sheet and Rill Erosion on Forest Land. USDA Forest Service, Atlanta, GA. Tech. Publ. No. SA-TP-11.

Dlamini, P., Orchard, C., Jewitt, G., Lorentz, S., Titshall, L., Chaplot, V., 2011. Controlling factors of sheet erosion under degraded grasslands in the sloping lands of KwaZulu-Natal, South Africa. Agr. Water Manage 98, 1711–1718. https://doi.org/10.1016/j.agwat.2010.07.016.

Dun, S.H., Wu, J.Q., Elliot, W.J., Robichaud, P.R., Flanagan, D.C., Frankenberger, J.R., Brown, R.E., Xu, A.C., 2009. Adapting theWater erosion prediction Project (WEPP) model for forest applications. J. Hydrol. 366, 46–54. https://doi.org/10.1016/j.jhydrol.2008.12.019.

Dunn, A.M., Julien, G., Ernst, W.R., Cook, A., Doe, K.G., Jackman, P.M., 2011. Evaluation of buffer zone effectiveness in mitigating the risks associated with agricultural runoff in Prince Edward Island. Sci. Total Environ. 409, 868–882. https://doi.org/10.1016/j.scitotenv.2010.11.011.

Elliot, W.J., 2004. WEPP Internet interfaces for forest erosion prediction. J. Am. Water Resour. Assoc. 40, 299–309. https://doi.org/10.1111/j.1752-1688.2004.tb01030.x.

Espigares, T., Heras, M., Nicolau, J., 2011. Performance of vegetation in reclaimed slopes affected by soil erosion. Restor. Ecol. 19, 35–44. https://doi.org/10.1111/j.1526-100X.2009.00546.x.

Foster, G.R., Huggins, L.F., Meyer, L.D., 1984. A laboratory study of rill hydraulics: II. Shear stress relationships. J. Tribol-T ASME 27, 797–804.

Gu, C., Mu, X., Gao, P., Zhao, G.J., Sun, W.Y., Tan, X.J., 2020. Distinguishing the effects of vegetation restoration on runoff and sediment generation on simulated rainfall on t he hillslopes of the loess plateau of China. Plant Soil 447, 393–412. https://doi.org/10.1007/s11104-019-04392-4.

Gyssels, G., Poesen, J., Bochet, E., Li, Y., 2005. Impact of plant roots on the resistance of soils to erosion by water: a review. Prog. Phys. Geogr. 29, 189–217.

Han, D.D., Deng, J.C., Gu, C.J., Mu, X.M., Gao, P., Gao, J.J., 2021. Effect of shrub-grass vegetation coverage and slope gradient on runoff and sediment yield under simulated rainfall. Int. J. Sediment Res. 36, 29–37. https://doi.org/10.1016/j.ijsrc.2020.05.004.

Hao, H.X., Guo, Z.L., Wang, X.Z., Zhan, H.G., Ma, R.M., Li, Z.X., Jiang, J., 2017. Rill erosion process on red soil slope under interaction of rainfall and scouring flow. Trans. CSAE 33, 134–140. https://doi.org/10.11975/j.issn.1002-6819.2017.08.018 (In Chinese).

Hou, J., Fu, B., Wang, S., Zhu, H., 2014. Comprehensive analysis of relationship between vegetation attributes and soil erosion on hillslopes in the Loess Plateau of China. Environ. Earth Sci. 72, 1721–1731. https://doi.org/10.1007/s12665-014-3076-1.

Huang, Z., Chen, L., Fu, B., Lu, Y., Huang, A., Gong, J., 2006. The relative efficiency of four representative cropland conversions in reducing water erosion: evidence from longterm plots in the Loess Plateau, China. Land Degrad. Dev. 17, 615–627. https://doi.org/10.1002/ldr.739.

Huo, Y., Bi, H., Zhu, Y., Xu, H., Wang, X., Chang, Y., 2015. Characteristics of artificial rainfall produced by QYJY-503C simulation system. Sci. Soil Water Conserv 13, 31–36. https://doi.org/10.3969/j.issn.1672-3007.2015.02.005 (In Chinese).

Iuss Working Group Wrb, 2015. World Reference Base for Soil Resources 2014, Update 2015. International Soil Classification System for Naming Soils and Creating Legends for Soil Maps. FAO, Rome. World Soil Resources Reports.

Kervroëdan, L., Armand, R., Mathieu, S., Ouvry, J., Faucon, M., 2018. Plant functional trait effects on runoff to design herbaceous hedges for soil erosion control. Ecol. Eng. 118, 143–151. https://doi.org/10.1016/j.ecoleng.2018.04.024.

Kim, K.H., Miller, W.P., 1996. Effect of rainfall electrolyte concentration and slope on infiltration and erosion. Soil Technol. 9, 173–185. https://doi.org/10.1016/S0933-3630(96)00011-6.

Krause, S., Lewandowski, J., Grimm, N.B., Hannah, D.M., Pinay, G., McDonald, K., Martí, E., Argerich, A., Pfister, L., Klaus, J., Battin, T., Larned S, T., Schelker, J., Fleckenstein, J., Schmidt, C., Rivett M, O., Watts, G., Sabater, F., Sorolla, A., Turk, V., 2017. Ecohydrological interfaces as hot spots of ecosystem processes. Water Resour. Res. 53, 6359–6376. https://doi.org/10.1002/2016WR019516.

Li, G., Abrahams, A.D., Atkinson, J.F., 1996. Correction factors in the determination of mean velocity of overland flow. Earth Surf. Proc. Land 21, 509–515. https://doi.org/10.1002/(SICI)1096-9837(199606)21:6<509::AID-ESP613>3.0.CO;2-Z.

Li, H.T., Zhao, Y.J., Li, G.R., Hu, X.S., Lu, H.J., Zhu, H.L., 2014. Experimental research on slope protection with vegetation under situ rainfall simulation in cold and arid environment of loess area. Res. Soil Water Conserv. 6, 304–311 (In Chinese).

Li, M., Yao, W., Ding, W., Yang, J., Chen, J., 2009. Effect of grass coverage on sediment yield in the hillslope-gully side erosion system. J. Geogr. Sci. 19, 321–330. https://doi.org/10.1007/s11442-009-0321-8.

Li, P., Cai, W., Zheng, L., Ru, H., 2006. Effects of vegetative cover on runoff hydraulic characteristics and erosion. Sci. Soil Water Conserv 4, 55–59. https://doi.org/10.3969/j.issn.1672-3007.2006.01.010.

Li, T.Y., He, B.H., Wang, R.X., Chen, Z.P., Zhang, Y., Liang, C., Zhao, P., 2017. Comparison of hydrodynamic parameters for predicting soil and water loss on simulation landslide deposit slope in Wenchuan earthquake area, China. Environ. Earth Sci. 76, 167. https://doi.org/10.1007/s12665-017-6462-7.

Li, X., Niu, X., Wang, B., Gao, P., Liu, Y., 2016. Driving forces of dynamic changes in soil erosion in the dahei mountain ecological restoration area of northern China based on GIS and RS. PLoS One 11, e0142331. https://doi.org/10.1371/journal.pone.0142331.

Lin, J.S., Zhu, G.L., Wei, J., Jiang, F.S., Wang, M.K., Huang, Y.H., 2018. Mulching effects on erosion from steep slopes and sediment particle size distributions of gully colluvial deposits. Catena 160, 57–67. https://doi.org/10.1016/j.catena.2017.09.003.

Liu, J.B., Gao, G.Y., Wang, S., Jiao, L., Wu, X., Fu, B.J., 2018. The effects of vegetation on runoff and soil loss:multidimensional structure analysis and scale characteristics. J. Geogr. Sci. 28, 59–78. https://doi.org/10.1007/s11442-018-1459-z.

Liu, Y.F., Liu, Y., Wu, G.L., Shi, Z.H., 2019. Runoff maintenance and sediment reduction of different grasslands based on simulated rainfall experiments. J. Hydrol 572, 329–335. https://doi.org/10.1016/j.jhydrol.2019.03.008.

Liu, Y.J., Wang, T.W., Cai, C.F., Li, Z., Cheng, D.B., 2014. Effects of vegetation on runoff generation, sediment yield and soil shear strength on road-side slopes under a simulation rainfall test in the Three Gorges Reservoir Area, China. Sci. Total Environ. 485–486, 93–102. https://doi.org/10.1016/j.scitotenv.2014.03.053.

Mahmoodabadi, M., Sajjadi, S.A., 2016. Effects of rain intensity, slope gradient and particle size distribution on the relative contributions of splash and wash loads to rain-induced erosion. Geomorphology 253, 159–167. https://doi.org/10.1016/j.geomorph.2015.10.010.

Mann, M.E., Lloyd, E.A., Oreskes, N., 2017. Assessing climate change impacts on extreme weather events: the case for an alternative (Bayesian) approach. Climatic Change 144, 131–142. https://doi.org/10.1007/s10584-017-2048-3.

Martínez-Murillo, J.F., Nadal-Romero, E., Regüés, D., Cerdà, A., Poesen, J., 2013. Soil erosion and hydrology of the western Mediterranean badlands throughout rainfall simulation experiments: a review. Catena 106, 101–112. https://doi.org/10.1016/j.catena.2012.06.001.

Mohammad, A.G., Adam, M.A., 2010. The impact of vegetative cover type on runoff and soil erosion under different land uses. Catena 81, 97–103. https://doi.org/10.1016/j.catena.2010.01.008.

Mu, H., Yu, X., Fu, S., Yu, B., Liu, Y., Zhang, G., 2019. Effect of stem cover on hydraulic parameters of overland flow. J. Hydrol 577, 123964. https://doi.org/10.1016/j.jhydrol.2019.123964.

Palucis, M.C., Ulizio, T.P., Fuller, B., Lamb, M.P., 2018. Flow resistance, sediment transport, and bedform development in a steep gravel-bedded river flume. Geomorphology 320, 111–126. https://doi.org/10.1016/j.geomorph.2018.08.003.

Pan, D., Gao, X., Dyck, M., Song, Y., Wu, P., Zhao, X., 2017. Dynamics of runoff and sediment trapping performance of vegetative filter strips: run-on experiments and modeling. Sci. Total Environ. 593, 54–64. https://doi.org/10.1016/j.scitotenv.2017.03.158.

Papanicolaou, A.N., Abban, B.K., Dermisis, D.C., Giannopoulos, C.P., Flanagan, D.C., Frankenberger, J.R., Wacha, K.M., 2018. Flow resistance interactions on hillslopes with heterogeneous attributes: effects on runoff hydrograph characteristics. Water Resour. Res. 54, 359–380. https://doi.org/10.1002/2017WR021109.

Pizarro, R., Araya, S., Jordán, C., Farias, C., Flores, J.P., Bro, P.B., 2006. The effects of changes in vegetative cover on river flows in the Purapel river basin of central Chile. J. Hydrol 327, 249–257. https://doi.org/10.1016/j.jhydrol.2005.11.020.

Qu, S.M., Wang, T., Bao, W.M., Shi, P., Jiang, P., Zhou, M.M., Yu, Z.B., 2013. Evaluating infiltration mechanisms using breakthrough curve and mean residence time. Water Resour. Manag. 27, 4579–4590. https://doi.org/10.1007/s11269-013-0427-8.

Ruiz-Colmenero, M., Bienes, R., Eldridge, D.J., Marques, M.J., 2013. Vegetation cover reduces erosion and enhances soil organic carbon in a vineyard in the central Spain. Catena 104, 153–160. https://doi.org/10.1016/j.catena.2012.11.007.

Sirjani, E., Mahmoodabadi, M., 2014. Effects of sheet flow rate and slope gradient on sediment load. Arab. J. Geosci 7, 203–210. https://doi.org/10.1007/s12517-012-0728-x.

Sun, W., Ma, X., Gao, P., Zhao, G., Chiew, F., 2019. Landscape patches influencing hillslope erosion processes and flow hydrodynamics. Geoderma 353, 391–400. https://doi.org/10.1016/j.geoderma.2019.07.003.

Vahabi, J., Nikkami, D., 2008. Assessing dominant factors affecting soil erosion using a portable rainfall simulator. Int. J. Sediment Res. 23, 376–386. https://doi.org/10.1016/S1001-6279(09)60008-1.

Wang, B., Niu, J.Z., Berndtsson, R., Zhang, L., Chen, X.W., Li, X., Zhu, Z.J., 2021. Efficient organic mulch thickness for soil and water conservation in urban areas. Sci. Rep. 11, 6259. https://doi.org/10.1038/s41598-021-85343-x.

Wang, C., Zhen, S., Wang, P., Hou, J., 2015. Interactions between vegetation, water flow and sediment transport: a review. J. Hydrodyn. 27, 24–37. https://doi.org/10.1016/S1001-6058(15)60453-X.

Wang, J., Zhang, K., Yang, M., Meng, H., Li, P., 2019. The effect of roughness and rainfall on hydrodynamic properties of overland flow. Hydrol. Res 50, 1324–1343. https://doi.org/10.2166/nh.2019.261.

Wang, S.P., Zhang, Z.Q., McVicar, T.R., Zhang, J.J., Zhu, J.Z., Guo, J.T., 2012. An event-based approach to understanding the hydrological impacts of different land uses in semi-arid catchments. J. Hydrol 416–417, 50–59. https://doi.org/10.1016/j.jhydrol.2011.11.035.

Wei, W., Chen, L., Fu, B., Huang, Z.L., Wu, D.P., Gui, L.D., 2007. The effect of land uses and rainfall regimes on runoff and soil erosion in the semi-arid loess hilly area, China. J. Hydrol 35, 247–258. https://doi.org/10.1016/j.jhydrol.2006.11.016.

Wei, W., Jia, F., Yang, L., Chen, L., Zhang, H., Yu, Y., 2014. Effects of surficial condition and rainfall intensity on runoff in a loess hilly area, China. J. Hydrol 513, 115–126. https://doi.org/10.1016/j.jhydrol.2014.03.022.

Wu, S., Wu, P., Feng, H., Li, M., 2007. Effects of forage grass on the reduction of runoff and sediment and the hydrodynamic characteristic mechanism of slope runoff in the standard slope plot. J. Beijing For. Univ. 29, 99–104. https://doi.org/10.3321/j.issn:1000-1522.2007.03.016.

Wu, X., Wei, Y., Wang, J., Xia, J., Cai, C., Wu, L., Fu, Z., Wei, Z., 2017. Effects of erosion degree and rainfall intensity on erosion processes for Ultisols derived from quaternary red clay. Agr. Ecosyst. Environ 249, 226–236. https://doi.org/10.1016/j.agee.2017.08.023.

Xiao, P.Q., Yao, W.Y., Shen, Z.Z., 2011b. Experimental study on erosion process and hydrodynamics mechanism of alfalfa grassland. J. Hydraul. Eng. 42, 232–237 (In Chinese).

Xiao, P.Q., Yao, W.Y., Shen, Z.Z., Yang, C.X., 2011a. Experimental study of critical flow energy for slope erosion under the influence of vegetation cover. Adv. Water Sci. 22, 229–234 (In Chinese).

Xiao, P.Q., Yao, W.Y., Shen, Z.Z., Yang, C.X., Lyu, X.Z., Jiao, P., 2017. Effects of shrub on runoff and soil loss at Loess Slopes under simulated rainfall. Chinese Geogr. Sci 27, 589–599. https://doi.org/10.1007/s11769-017-0889-3.

Xin, Y., Xie, Y., Liu, Y.X., Liu, H.Y., Ren, X.Y., 2016. Residue cover effects on soil erosion and the infiltration in black soil under simulated rainfall experiments. J. Hydrol 543, 651–658. https://doi.org/10.1016/j.jhydrol.2016.10.036.

Xu, M.Y., Xie, F., Li, Y.Q., Guo, M., Li, Y.Q., Liang, J.F., Aotegen, B.Y., 2006a. The rangeland type and current situation of Chongli county in sand source areas around Beijing and Tianjin. J. Agric. Univers. Hebei 29, 72–76 (In Chinese).

Xu, X.L., Ma, K.M., Fu, B.J., Liu, X.C., Huang, Y., Qi, J., 2006b. Research review of the relationship between vegetation and soil loss. Acta Ecol. Sin. 26, 3137–3143. https://doi.org/10.3321/j.issn:1000-0933.2006.09.044.

Xu, X., Zheng, F., Qin, C., Wu, H., Wilson, G.V., 2017. Impact of cornstalk buffer strip on hillslope soil erosion and its hydrodynamic understanding. Catena 149, 417–425. https://doi.org/10.1016/j.catena.2016.10.016.

Yan, Y., Dai, Q., Yuan, Y., Peng, X., Zhao, L., Yang, J., 2018. Effects of rainfall intensity on runoff and sediment yields on bare slopes in a karst area, SW China. Geoderma 330, 30–40. https://doi.org/10.1016/j.geoderma.2018.05.026.

Yang, F., Zhang, K.D., Yang, M.Y., Wang, J.J., 2016. Experimental study on hydraulic characteristics of flow under vegetation stem. J. Sediment. Res. 4, 22–27. https://doi.org/10.16239/j.cnki.0468-155x.2016.04.004.

Yao, W.Y., Xiao, P.Q., Shen, Z.Z., Yang, C.X., 2011. Responses of runoff process and threshold of sediment generation for different vegetation-covered plot. J. Hydraul. Eng. 42, 1438–1444 (In Chinese).

Yao, Y.F., Zhu, H.L., Zhang, L.H., Yan, C.Y., 2013. Influence of rainfall electrolyte concentration on water and soil migration characteristics. J. Soil Water Conserv. 27, 44–48 (In Chinese).

Yu, G.Q., Li, Z.B., Li, P., Zhang, X., Chen, L., Jia, L.L., 2010. Effects of vegetation types on hillslope runoff-erosion and sediment yield. Adv. Water Sci. 21, 593–599 (In Chinese).

Zare, M., Samani, A.A.N., Mohammady, M., Teimurian, T., Bazrafshan, J., 2016. Simulation of soil erosion under the influence of climate change scenarios. Environ. Earth Sci. 75, 1405. https://doi.org/10.1007/s12665-016-6180-6.

Zhang, C.S., Xie, G.D., Liu, C.L., Lu, C.X., 2011. Assessment of soil erosion under woodlands using USLE in China. Front. Earth Sci. 5, 150–161. https://doi.org/10.1007/s11707-011-0158-1.

Zhang, J.Z., Zhang, S.T., Chen, S., Liu, M., Xu, X.F., Zhou, J.S., Wang, W.J., Ma, L.J., Wang, C.T., 2021. Overland flow resistance law under sparse stem vegetation coverage. Water 13, 1657. https://doi.org/10.3390/w13121657.

Zhang, K.D., Wang, Z.G., Wang, G.Q., Sun, X.M., Cui, N.B., 2017. Overland-flow resistance characteristics of nonsubmerged vegetation. J Irrig. Drain. E-ASCE 143, 04017021. https://doi.org/10.1061/(ASCE)IR.1943-4774.0001196.

Zhang, K., Wang, G., Sun, X., Wang, J., 2014a. Hydraulic characteristic of overland flow under different vegetation coverage. Adv. Water Sci. 25, 825–834 (In Chinese).

Zhang, L.T., Gao, Z.L., Tian, H.W., 2013. Hydrodynamic process of soil erosion in steep slope of engineering accumulation. Trans. CSAE 29, 94–102. https://doi.org/10.3969/j.issn.1002-6819.2013.24.013.

Zhang, L.T., Gao, Z.L., Yang, S.W., Li, Y.H., Tian, H.W., 2015. Dynamic processes of soil erosion by runoff on engineered landforms derived from expressway construction: a case study of typical steep spoil heap. Catena 128, 108–121. https://doi.org/10.1016/j.catena.2015.01.020.

Zhang, Q.L., Wang, Z.L., Wang, D.D., Liu, J.E., 2017a. Advances in researches of the effects of grassland vegetation on soil erosion in loess plateau. Adv. Earth Sci. 32, 1093–1101. https://doi.org/10.11867/j.issn.1001-8166.2017.10.1093.

Zhang, X., Liang, J., Yu, S., Du, H., Wen, H.D., 2017b. Analysis of the distribution characteristics of soil nutrients of mountain slope in qingshui river watershed. J. Agric. Univers. Hebei 40, 27–38 (In Chinese).

Zhang, X., Yu, G.Q., Li, Z.B., Li, P., 2014b. Experimental study on slope runoff, erosion and sediment under different vegetation types. Water Resour. Manag. 28, 2415–2433. https://doi.org/10.1007/s11269-014-0603-5.

Zhang, Z.Q., Wang, S.P., Sun, G., Xie, B.Y., 2006. Runoff and sediment yield response to vegetation change at multiple scales: a review. Acta Ecol. Sin. 26, 2356–2364. https://doi.org/10.3321/j.issn:1000-0933.2006.07.039.

Zhao, B.Q., Zhang, L., Xia, Z.Y., Xu, W.N., Xia, L., Liang, Y.Z., Xia, D., 2019. Effects of rainfall intensity and vegetation cover on erosion characteristics of a soil containing rock fragments slope. Adv. Civ. Eng. 2019, 7043428. https://doi.org/10.1155/2019/7043428.

Zhou, P., Luukkanen, O., Tokola, T., Nieminen, J., 2008. Effect of vegetation cover on soil erosion in a mountainous watershed. Catena 75, 319–325. https://doi.org/10.1016/j.catena.2008.07.010.

Zhu, B.B., Li, Z.B., Li, P., You, Z., 2010. Effect of grass coverage on sediment yield of rain on slope. Acta Pedol. Sin. 47, 401–407 (In Chinese).

Zuazo, V.H.D., Pleguezuelo, C.R.R., 2008. Soil-erosion and runoff prevention by plant covers: a review. Agron. Sustain. Dev. 28, 65–86. https://doi.org/10.1051/agro:2007062.